energies

MDPI

Article

Adaptive Droop Based Virtual Slack Control of Multiple DGs in Practical DC Distribution System to Improve Voltage Profile

Soo Hyoung Lee

Department of Electrical and Control Engineering, Mokpo National University (MNU), 1666, Yeongsan-ro, Cheonggye-myeon, Muan-gun, Jeollanam-do 58554, Korea; slee82@mokpo.ac.kr; Tel.: +82-61-450-2751

Received: 20 February 2019; Accepted: 22 April 2019; Published: 24 April 2019

Abstract: This paper proposes an adaptive droop based virtual slack (ADVS) control for multiple distributed generations (DGs) to improve voltage stability of a practical DC distribution system. Although there have been many researches for optimal sizes of multiple DGs, their solutions are valid only in the particular operating point. Additionally, a previous study proposed a voltage control based optimal operation method, its performance depends on measurement accuracy in practice. The proposed ADVS control operates the system based on the current sensitivities between the DGs and loads, so that it can regulate the system voltages without a large computational effort. This is effective even if measurements are noisy and biased. All DGs contribute to voltage regulation by current control even though they do not directly control voltages. As an additional effect, they effectively share the load. To verify the proposed method, the DC system is modeled based on the real distribution system of the Do-gok area in Seoul, Korea. Then, the Levenberg-Marquardt algorithm determines its operation point. The proposed method is verified based on the electromagnetic transient (EMT) simulation with random loads.

Keywords: adaptive droop; current sensitivity; direct current distribution; Levenberg-Marquardt algorithm; on-line estimation; virtual slacks

1. Introduction

Currently, electric power systems are facing huge challenges of being environment-friendly worldwide. For example, the Korean government has planned to increase renewable energies up to 20% of the entire power generation by 2030 instead of constructing a new conventional power plant. Additionally, constructing new infrastructures such as transmission lines is facing socio-economic issues. Therefore, the electric power systems are not only toward maximum utilization of existing infrastructures with tight operating margins, but also toward decentralized small-scale grids including distributed generations (DGs).

In most cases, the DGs take the form of converter-based- generators (CBGs). For example, the fuel cell and photovoltaic supply power through DC-to-AC converters. The other DGs such as wind and micro gas/hydro turbines synchronize their outputs to grid by back-to-back converters. In addition, a battery energy storage system (BESS) charges/discharges the DC power. Moreover, a lot of electronic devices result in an increase of DC loads. As a result, the efficiency of the existing AC power system is aggravated due to the losses caused by numerous power conversions. This problem can be alleviated by introducing DC power systems that minimize the numbers of the power conversions.

The DC power systems can improve the voltage stability and power efficiency. Note that the AC systems have a larger current than the DC systems if their load consumptions are the same. In addition, AC systems have larger impedances than DC systems due to the inductive components. Therefore,

the voltage drops in the AC systems are larger than those in the DC systems. Capacitor banks that inject reactive powers usually restore the voltage drops in the AC systems. In the same manner, the DGs can improve the voltage profile by injecting reactive powers. Meanwhile, the rated current limits the maximum apparent powers of the CBGs. Therefore, the reactive power injections might cause insufficient real power injections in a full load condition. In contrast, the DC systems are intrinsically free from the reactive power related problems.

There have been several studies related to the DC systems; device and control [1–9], management [10–12], cable and power conversion [13–16], DC distribution test-bed [17,18], and optimal DG sizing [19–23]. Although the optimal operation method [24] makes the multiple DGs properly share the loads as well as instantly respond to the load variations, the DGs must control their output voltages very accurately to do this.

In practice, the measurement error in the voltage has a much more significant effect on power flow than that in current. This is because resistance of the transmission line is generally very small. This paper introduces the adaptive droop based virtual slack (ADVS) control of multiple DGs, which indirectly controls the voltage by current control. As a result, the DC distribution system can be robust to the voltage measurement error while its voltages are kept in constant.

This paper is organized as follows: Section 2 describes the control issues in the DC power system. Section 3 explains the DC distribution system operation. Then, several case studies are carried out in Section 4. Finally, the conclusions are given in Section 5.

2. Control Issues in DC Power System

2.1. Voltage Control of DG

Unit circuits representing the steady state the AC and DC system are shown in Figure 1. The AC circuit includes both resistance and reactive components. In contrast, the DC circuit includes the only resistance. Assume that both unit circuits have the same effective resistance.

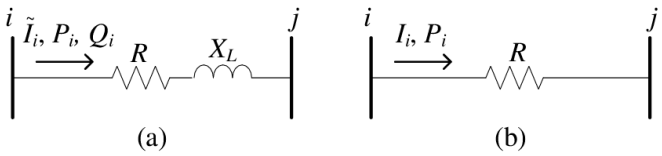

Figure 1. (**a**) AC and (**b**) DC unit circuits.

In the AC unit circuit, the real and reactive powers, P_i and Q_i are respectively determined by

$$P_i = \frac{V_i^2}{Z}\cos\gamma - \frac{V_i V_j}{Z}\cos(\gamma + \delta_i - \delta_j) \quad (1)$$

$$Q_i = \frac{V_i^2}{Z}\sin\gamma - \frac{V_i V_j}{Z}\sin(\gamma + \delta_i - \delta_j) \quad (2)$$

where V_i and δ_i are the magnitude and phase angle of the voltage in bus i, respectively. Also, Z and γ are the magnitude and phase angle of the line impedance. In general, the reactive impedance, X_L is much larger than the resistance, so that γ is almost $\pi/2$ radians. Additionally, δ_i–δ_j is generally a few degrees in the stable power system. In the case of fixed V_j and δ_j, therefore, the deviations of P_i and Q_i are dominantly determined by the deviations of δ_i and V_i, respectively [25]. In other words, P_i and δ_i cannot be controlled independently at the same time. This is the same for Q_i and V_i. As shown in Table 1, the slack generator determines V and f (i.e., time derivative of δ) while P and Q are given from the system. The other generator determines V and P while f and Q are given from the system. The load determines P and Q while V and δ are given from the system.

Table 1. AC and DC state variables determined by the device or given from the system

	AC		DC	
	Device	**System**	**Device**	**System**
Slack	V, f	P, Q	V	P
Generator	V, P	f, Q	P	V
Load	P, Q	V, δ	P	V

In the DC unit circuit, the power injection in bus i, P_i is determined by

$$P_i = \frac{V_i^2 - V_i V_j}{R} \tag{3}$$

where V_i and R are the voltage in bus i and line resistance, respectively. The relationship between the voltages and power is described by the derivative of (3) as

$$\frac{\partial P_i}{\partial V_i} = \frac{2V_i - V_j}{R} \tag{4}$$

where V_i and V_j are near 1 pu in normal condition. Therefore,

$$\frac{\partial P_i}{\partial V_i} \approx \frac{1}{R} \tag{5}$$

In general, R is very small and therefore P and V are highly coupled. In other words, P and V cannot be independently controlled in bus i. The slack generator determines V while P is given from the system. The other generator and load determines P, respectively, while V is given from the system.

Theoretically, all DGs can be operated in the voltage control mode to regulate the system voltages. In practice, however, the DG voltages might be different from their ideal values due to the measurement and control errors. The voltage errors might change the power flow significantly by (5). For example, assume that P_i is ideally 1 pu when the references of V_i and V_j are 1 pu and 0.99 pu, respectively, while R is 0.01 pu. In the case of 1% voltage errors, V_i and V_j can be worst 1.01 pu and 0.98 pu, respectively. Then, P_i becomes 3 pu (i.e., 200% of power error) and the line might be overloaded. In other words, the unintended power flow (i.e., current) might be occurred, so that the power system and the DGs might be damaged by the large current.

2.2. Power Control of DG

In the DC power system, the DGs are operated in the power control mode if they are not slack generators. Therefore, the entire system must be analyzed several times to determine proper powers of the DGs, which satisfy the voltage profile. The analysis starts from the simplified DC power system, which is composed with bus i and its adjacent buses, as shown in Figure 2.

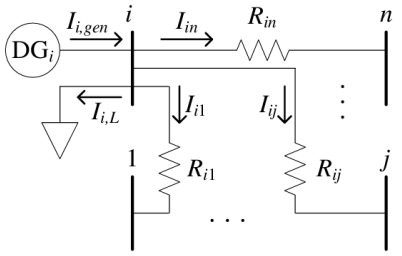

Figure 2. DC power system composed with bus i and its adjacent buses.

According to Kirchhoff's current law, the net current injection to bus i, I_i ($=I_{i,gen} - I_{i,L}$) is equal to the sum of currents to adjacent buses as

$$I_i = \sum_{j=1}^{n} I_{ij} = \sum_{j=1}^{n} \frac{V_i - V_j}{R_{ij}} = V_i \sum_{j=1}^{n} g_{ij} - \sum_{j=1}^{n} V_j g_{ij} \tag{6}$$

where n is the number of buses and $g_{ij} = 1/R_{ij}$. Then, the current injection vector can be represented as

$$\mathbf{I} = \mathbf{G} \cdot \mathbf{V} \tag{7}$$

where $\mathbf{I}$ ($\in \mathrm{R}^{n\times 1}$), $\mathbf{G}$($\in \mathrm{R}^{n\times n}$), and $\mathbf{V}$($\in \mathrm{R}^{n\times 1}$) are $[I_1 \cdot\cdot I_i \cdot\cdot I_n]^T$, $[[G_{11} \cdot\cdot G_{i1} \cdot\cdot G_{n1}]^T \cdot\cdot [G_{1i} \cdot\cdot G_{ii} \cdot\cdot G_{ni}]^T \cdot\cdot [G_{1n} \cdot\cdot G_{in} \cdot\cdot G_{nn}]^T]$, and $[V_1 \cdot\cdot V_i \cdot\cdot V_n]^T$, respectively. Here, G_{ii} and G_{ij} ($i \neq j$) are $\sum_{j=1}^{n} g_{ij}$ and $-g_{ij}$, respectively. Then, the power flow equation on bus i is formulated as

$$P_i = V_i \sum_{j=1}^{n} G_{ij} V_j = P_{i,gen} - P_{i,L} \tag{8}$$

Likewise with the AC system, the power flow of the DC system can be analyzed by using Newton's method. In contrast to the AC system, however, the Jacobian matrix of the DC system, $\mathbf{J}$ ($\in \mathrm{R}^{n\times n}$) consists of the partial derivatives of the only real powers with respect to the voltage magnitudes as

$$\mathbf{J} = \frac{\partial \mathbf{P}}{\partial \mathbf{V}} \tag{9}$$

In other words, the diagonal and off-diagonal elements of $\mathbf{J}$ are determined by

$$\frac{\partial P_i}{\partial V_i} = \sum_{j=1}^{n} V_j G_{ij} + V_i G_{ii} \tag{10}$$

$$\frac{\partial P_i}{\partial V_j} = V_i G_{ij}, \ (i \neq j) \tag{11}$$

A simple control procedure is shown in Figure 3 to determine the proper DG powers, which satisfy the voltage profile. First, the operator selected $P_{i,gen}$. Then, it is determined if $P_{i,gen}$ is between maximum and minimum powers of DG_i. If so, the powerflow is analyzed. Otherwise, $P_{i,gen}$ is adjusted before the powerflow analysis. Thereafter, it is determined if $I_{i,gen}$ is between maximum and minimum currents of DG_i. Finally, $P_{i,gen}$ is applied to DG_i if V_i satisfies the grid code of the voltage. As a result, the voltage profile can be satisfied even if most of the DGs control powers. However, the procedure requires a high computational effort. This is because it includes several feedback loops. Specifically, the procedure repeats the powerflow analysis that requires many iteration for itself. Consequently, the real-time operation becomes difficult.

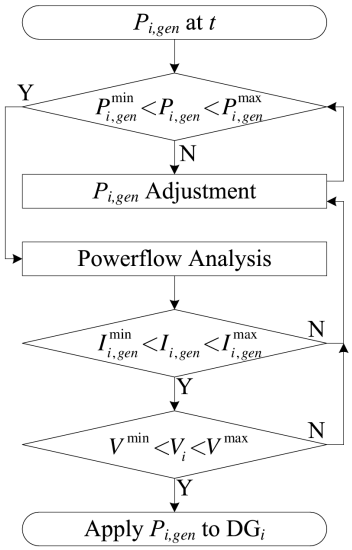

Figure 3. Power control procedure at each time step.

3. DC Distribution System Operations

For the computationally efficient operation, a DC distribution system operation method is proposed as shown in Figure 4. The DC distribution system is modeled based on the real distribution system in the Do-gok area, Korea. The proposed method operates the DC distribution system as follows.

- The system estimation block estimates the conductance matrix of the distribution system, **G**, and generates the current sensitivity matrix, $\partial \mathbf{I}_{gen,ref}/\partial \mathbf{I}_L$ between DGs and loads. **G** is estimated on-line, and supports decision making of the operator person.
- The optimal current flow block determines the offset current reference vector of the DGs, $\mathbf{I}_{gen,o}$. Also, it checks if the current reference vector, $\mathbf{I}_{gen,ref}$ exceeds the current limits of the DGs. If so, it adjusts $\mathbf{I}_{gen,o}$ to modify $\mathbf{I}_{gen,ref}$.
- The virtual slack control block generates $\mathbf{I}_{gen,ref}$ based on $\mathbf{I}_{gen,o}$ and $\partial \mathbf{I}_{gen,ref}/\partial \mathbf{I}_L$.

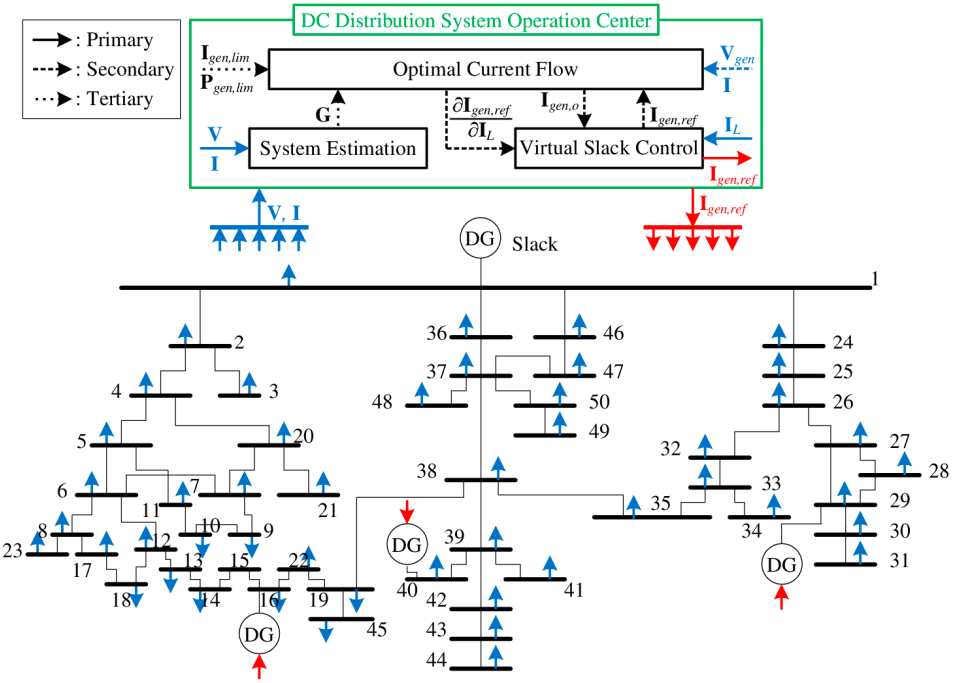

Figure 4. Practical DC distribution system based on real AC distribution system in the Do-gok area, Korea.

3.1. Optimal Current Flow

3.1.1. Current Flow Analysis

To minimize the computational effort, the power flow of (8) is modified to a current flow as

$$I_i = \sum_{j=1}^{n} G_{ij} V_j = I_{i,gen} - I_{i,L} \tag{12}$$

In the same manner with the power flow, the current flow can be analyzed by using Newton's method. From (7), the Jacobian matrix is derived to

$$\mathbf{J}_{IV} = \frac{\partial \mathbf{I}}{\partial \mathbf{V}} = \mathbf{G} \tag{13}$$

Meanwhile, the difference between scheduled and calculated current injections is given by

$$\Delta \mathbf{I}^{(noi)} = \mathbf{I}^{sch} - \mathbf{I}^{(noi)} \tag{14}$$

where *noi* and *sch* are number of iterations and scheduled value, respectively. Then, the bus voltages are updated by

$$\mathbf{V}^{(noi+1)} = \mathbf{V}^{(noi)} + \mathbf{J}_{IV}^{-1} \cdot \Delta \mathbf{I}^{(noi)} \tag{15}$$

Update of $\mathbf{J}_{IV}$ ($\in \mathrm{R}^{n \times n}$) is not required during the current flow analysis. In other words, $\mathbf{G}$ can be considered as constant regardless of the values of the voltages and currents. This is because the computational time for the current flow analysis is relatively very short compared to the system topology or impedance variations. The constant $\mathbf{J}_{IV}$ (i.e., linear system) makes the solution converges within a few iterations. As the result, the computational effort is dramatically reduced by using the current flow instead of the power flow.

3.1.2. Optimal Current Flow with Constraints

Thanks to the beneficial effect of the constant Jacobian matrix, the optimal condition of the system can be determined by the optimal current flow (OCF) analysis with a small computational effort. For the OCF analysis, the Levenberg-Marquardt (L-M) algorithm [26] is applied. The L-M algorithm is the combined type of gradient descent and Gauss-Newton algorithms. It updates the parameters adaptively by

$$(\mathbf{A}^{\mathrm{T}}\mathbf{A} + \mu \mathbf{U})\boldsymbol{\delta} = \mathbf{A}^{\mathrm{T}}[\mathbf{y} - \mathrm{f}(\boldsymbol{\beta})] \tag{16}$$

where $\mathbf{U}$ ($\in \mathrm{R}^{n \times n}$) is the identity matrix, parameter μ is the damping factor, and parameter $\mathbf{y}$ ($\in \mathrm{R}^{n \times 1}$) is set to the normal voltage (i.e., 1 pu in general). $\mathrm{f}(\boldsymbol{\beta})$ ($\in \mathrm{R}^{n \times 1}$) is the same with $\boldsymbol{\beta}$ that composed of bus voltages as

$$\boldsymbol{\beta} = [V_1, \cdots, V_i, \cdots, V_n]^T \tag{17}$$

Then, $\boldsymbol{\beta}$ is updated by vector $\boldsymbol{\delta}$ ($\in \mathrm{R}^{n \times 1}$). The modified Jacobian matrix, $\mathbf{A}$ ($\in \mathrm{R}^{n \times n}$) is composed of

$$A_{ij} = \varepsilon_i B_{ij} \tag{18}$$

where

$$B_{ij} = \frac{\partial V_i}{\partial V_j} \tag{19}$$

To determine ε_i, a temporary update is performed by

$$(\mathbf{B}^{\mathrm{T}}\mathbf{B} + \mu \mathbf{U})\boldsymbol{\delta} = \mathbf{B}^{\mathrm{T}}[\mathbf{y} - \mathrm{f}(\boldsymbol{\beta})] \tag{20}$$

Then, a temporary deviation of currents and powers are calculated by

$$\Delta I_{i,gen}^{tmp} = I_{i,gen}^{(noi+1)} - I_{i,gen}^{(noi)} \tag{21}$$

$$\Delta P_{i,gen}^{tmp} = P_{i,gen}^{(noi+1)} - P_{i,gen}^{(noi)} \tag{22}$$

Thereafter, ε_i^x ($x = I$ or P) is determined by

$$\varepsilon_i^x = \begin{Bmatrix} \frac{\left(x_{i,gen}^{\max} - x_{i,gen}^{\text{high}}\right)}{\left(x_{i,gen}^{\max} - x_{i,gen}\right)}, x_{i,gen} \geq x_{i,gen}^{\text{high}} \& \Delta x_{i,gen}^{tmp} \geq 0 \\ \frac{\left(x_{i,gen}^{\text{low}} - x_{i,gen}^{\min}\right)}{\left(x_{i,gen} - x_{i,gen}^{\min}\right)}, x_{i,gen} \leq x_{i,gen}^{\text{low}} \& \Delta x_{i,gen}^{tmp} \leq 0 \\ 1 \qquad\qquad , \text{otherwise} \end{Bmatrix} \tag{23}$$

where $x^{\text{low}}/x^{\min}$ and $x^{\text{high}}/x^{\max}$ are starting/ending points of lower and upper boundaries, respectively. Finally, ε_i is determined by

$$\varepsilon_i = \frac{\left(\varepsilon_i^I + \varepsilon_i^P\right)}{2} \tag{24}$$

The temporary update is only used to determine ε_i. An authentic update is conducted by (16). As a result, ε_i prevents the $x_{i,gen}$ moving toward out of the boundary. Performance of the OCF is evaluated by

$$\sigma_V = \sqrt{\frac{\sum_{i=1}^{n} \left(V_i - V_{normal}\right)^2}{n}} \tag{25}$$

where V_{normal} is the normal voltage, which is used for $\mathbf{y}$ in (16).

As a result of OCF, voltage targets of DGs are adjusted to make margins to the power/ current limitations. Consider, for example, a DG requires supplying 50 A to maintain 22.9 kV. Additionally, assume that the DG needs to supply 45 A to maintain 22.7 kV. If the DG has 45 A limitation, the DG cannot play the role of slack generator while maintaining 22.9 kV. In this case, the OCF makes the DG operate in 40 A and 22.5 kV to secure some margins. As a result, the DG can emulate a slack generator by controlling its current according to the network conditions.

3.2. Virtual Slack Control Based on Adaptive Droop

For the frequency regulation in the AC system, the rotor of the generator releases or absorbs inertial power first according to the frequency derivative during the arresting period. Next, the governor free (G/F) operation adjusts the power by responding to the frequency deviation during the rebound period. After that, the automatic generator control (AGC) balances the power of the entire system to recover the rated frequency during the recovery period. In the DC system, similarly, the capacitor releases or absorbs power first according to the voltage derivative. As described in Section 2.1, however, the control based on voltage measurement might not be feasible in practice. To solve this, the ADVS control is proposed as follows.

First, a resistance matrix is calculated as

$$\mathbf{R} = \mathbf{G}^{-1} \tag{26}$$

Then, a relationship between voltage and current deviations can be derived as

$$\Delta \mathbf{V} = \mathbf{R} \cdot \Delta \mathbf{I} \tag{27}$$

Thereafter, the voltages deviations in the DG connected buses can be derived as

$$\Delta \mathbf{V}_{gen} = \mathbf{R}_{gen} \cdot \Delta \mathbf{I}_{gen} - \mathbf{R}_{gen,row} \cdot \Delta \mathbf{I}_L \tag{28}$$

where $\mathbf{R}_{gen}$ ($\in \mathrm{R}^{m \times m}$) is composed of R_{ij}, which is ith row and jth column component of $\mathbf{R}$, when buses i and j have DGs. $\mathbf{R}_{gen,row}$ ($\in \mathrm{R}^{m \times n}$) is composed of $\mathbf{R}_i$, which is ith row vector, when bus i has a DG. $\Delta \mathbf{I}_{gen}$ is the DG currents deviations vector, and $\Delta \mathbf{I}_L$ is the load currents deviations vector. For an ideal voltage control of the DGs, DG voltages deviations vector, ΔV_{gen} must be zero. Therefore, $\Delta \mathbf{I}_{gen}$ is determined by

$$\Delta \mathbf{I}_{gen} = \mathbf{R}_{gen}^{-1} \cdot \mathbf{R}_{gen,row} \cdot \Delta \mathbf{I}_L \tag{29}$$

where each entry of $\mathbf{R}_{gen}^{-1} \cdot \mathbf{R}_{gen,row}$ represents the droop between generation and load currents. The droop values are adaptively determined by the on-line conductance matrix estimation that is described in next Section 3.3.

Equation (29) can be extended to (30) because $\mathbf{I}_L = \mathbf{0}$ results in $\mathbf{I}_{gen} = \mathbf{0}$, and the resistances are constant.

$$\mathbf{I}_{gen} = \mathbf{R}_{gen}^{-1} \cdot \mathbf{R}_{gen,row} \cdot \mathbf{I}_L \tag{30}$$

Therefore, required DG currents can be determined from measured load currents without a huge computational effort, which is required for the powerflow analysis. If a power shortage is expected for a particular DG, the operating point can be changed by inserting offset currents, $\mathbf{I}_{gen,o}$ as

$$\mathbf{I}_{gen,ref} = \mathbf{I}_{gen,o} + \mathbf{R}_{gen}^{-1} \cdot \mathbf{R}_{gen,row} \cdot \mathbf{I}_L \tag{31}$$

To sum up, OCF performs the AGC role by determining $\mathbf{I}_{gen,o}$.

3.3. On-Line Conductance Matrix Estimation Using Kalman-Filter Algorithm

The DC distribution system model is implemented based on the manufacturer given parameters at first. There might be an error between the model and the real system necessarily because of several reasons. First, for example, the given parameters have an error. In addition, the parameters of the real system are affected by circumstances, such as temperature, solar radiation, wind speed, and aging, etc. To deal with this problem, the on-line conductance matrix estimation algorithm is studied based on the Kalman-filter algorithm. The Kalman-filter algorithm [27,28] has the smoothing properties and the noise rejection capability robust to the process and measurement noises. In practical environments (in which the states are driven by process noise and observation is made in the presence of the measurement noise), the on-line estimation problem for the conductance matrix of the n bus system can be formulated with a *linear time-varying* state equation. In this study, the state model applied for the estimation is given as

$$\begin{gathered} \mathbf{x}(t + \Delta t) = \mathbf{\Phi x}(t) + \mathbf{\Gamma \omega}(t), \mathbf{x}(0) = \mathbf{x}_0 \\ \mathbf{y}(t) = \mathbf{c}(t) \cdot \mathbf{x}(t) \\ \mathbf{z}(t) = \mathbf{y}(t) + \mathbf{v}(t) \end{gathered} \tag{32}$$

where the matrices, $\mathbf{\Phi}$ ($\in \mathrm{R}^{n \times n}$), $\mathbf{\Gamma}$ ($\in \mathrm{R}^{n \times m}$), and $\mathbf{c}$ ($\in \mathrm{R}^{1 \times n}$) are known deterministic variables, and the identity matrix, $\mathbf{I}$ ($\in \mathrm{R}^{n \times n}$), is usually chosen for the matrix, $\mathbf{\Phi}$. The state matrix, $\mathbf{x}$ ($\in \mathrm{R}^{n \times n}$) represents the conductance matrix. And, $\boldsymbol{\omega}$ ($\in \mathrm{R}^{m \times n}$) is the process noise vector, $\mathbf{z}$ ($\in \mathrm{R}^{1 \times n}$) is the measured output, and $\mathbf{v}$ ($\in \mathrm{R}^{1 \times n}$) is the stationary measurement noise. Then, the estimate of the state vector is updated by using the following steps:

- Measurement update: Acquire the measurements, $\mathbf{z}(t)$ and compute a *posteriori* quantities.

$$\begin{gathered} \mathbf{k}(t) = \mathbf{P}^-(t)\mathbf{c}(t)^T[\mathbf{c}(t)\mathbf{P}^-(t)\mathbf{c}(t)^T + r]^{-1} \\ \hat{\mathbf{x}}(t) = \hat{\mathbf{x}}^-(t) + \mathbf{k}(t)[\mathbf{z}(t) - \mathbf{c}(t)\hat{\mathbf{x}}^-(t)] \\ \mathbf{P}(t) = \mathbf{P}^-(t) - \mathbf{k}(t)\mathbf{c}(t)\mathbf{P}^-(t) \end{gathered} \tag{33}$$

where $\mathbf{k}$ ($\in \mathrm{R}^{n\times 1}$) is the Kalman gain, $\mathbf{P}$ ($\in \mathrm{R}^{n\times n}$) is a positive-definite symmetric matrix, and r is a positive number selected to avoid a singular matrix. Typically, $\mathbf{P}^{-}(0)$ is given as $\mathbf{P}^{-}(0) = \lambda\mathbf{I}$ ($\lambda > 0$), where $\mathbf{I}$ is an identity matrix.

- Time update:

$$\begin{aligned} \hat{\mathbf{x}}^{-}(t+\Delta t) &= \mathbf{\Phi}\hat{\mathbf{x}}(t) \\ \mathbf{P}^{-}(t+\Delta t) &= \mathbf{\Phi}\mathbf{P}(t)^{T} + \mathbf{\Gamma}\mathbf{Q}\mathbf{\Gamma}^{T} \end{aligned} \tag{34}$$

where $\mathbf{Q}$ ($\in \mathrm{R}^{m\times m}$) is a positive-definite covariance matrix, which is zero in this study because the stationary process and measurement noises are mutually independent.

- Time increment: Increment t and repeat.

Thereafter, the estimated output, $\hat{\mathbf{y}}$ ($\in \mathrm{R}^{1\times n}$) is calculated as

$$\hat{\mathbf{y}}(t) = \mathbf{c}(t) \cdot \hat{\mathbf{x}}(t) \tag{35}$$

The conductance matrix is estimated by the voltages and currents measured from all buses. The matrices, $\mathbf{c}(t)$ and $\mathbf{z}(t)$ are determined by

$$\mathbf{c}(t) = \mathbf{V}(t)^{T} \tag{36}$$

$$\mathbf{z}(t) = \mathbf{I}(t)^{T} \tag{37}$$

where the matrices $\mathbf{V}(t)$ and $\mathbf{I}(t)$ are composed of measured voltages and currents, respectively, from all buses throughout the entire time range of the measurement window. Next, the estimated state, $\hat{\mathbf{x}}(t)$ is determined by the Kalman-filter algorithm described in (33) and (34). After that, the conductance matrix is estimated by

$$\mathbf{G}(t) = \hat{\mathbf{x}}(t)^{T} \tag{38}$$

The accuracy of the estimated conductance matrix can be evaluated by

$$V_{\mathrm{RMSE}} = \sqrt{\frac{\sum_{i=1}^{n}\left(V_i^{cal}(t) - V_i^{meas}(t)\right)^2}{n}} \tag{39}$$

$$I_{\mathrm{RMSE}} = \sqrt{\frac{\sum_{i=1}^{n}\left(I_i^{cal}(t) - I_i^{meas}(t)\right)^2}{n}} \tag{40}$$

where V^{cal} and I^{cal} are obtained by the system analysis using the estimated conductance matrix. Other terms, V^{meas} and I^{meas} are measured voltage and current.

The conductance matrix can be estimated in real-time. This is because the resistances of the lines change very slowly in the real power system.

4. Case Studies

4.1. Optimal Current Flow

4.1.1. Current Flow Analysis

As described in Section 3.1, the DC current flow analysis converges within a few iterations thanks to the constant Jacobians while it has smaller maximum current deviations than the power flow analysis. For example, the current flow of the DC system in Figure 4 converges within five iterations as shown in Figure 5 with a critical deviation of 10^{-7} A. The convergence time is between 0.2 and 0.6 s using Intel i7-4510U CPU.

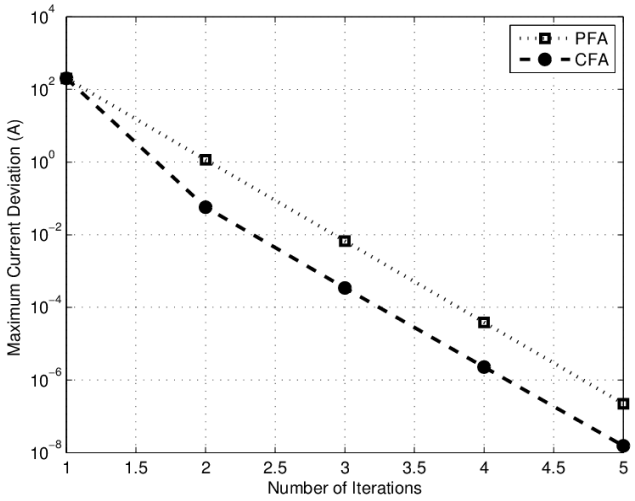

Figure 5. Maximum current deviation in log scale showing convergences of power flow analysis (PFA) and current flow analysis (CFA).

4.1.2. Optimal Current Flow with Constraints

To maximize the voltage profile, voltage deviation is selected as the objective function of the OCF. Therefore, the powers or currents of the OCF solution may exceed the capabilities of the DGs unless there are proper constraints during the OCF. For the constraints in DG_i, $P_i^{\max}$ and $I_i^{\max}$ are first set to 1100 kW and 50 A, respectively. Also, $P_i^{\min}$ and $I_i^{\min}$ are set to zeros. For the auxiliary constraints, P_i^{high} is set to 861.5 kW, which is one third of the average total load size, in consideration of four sources (i.e., P_i might be P_i^{high} if one DG is removed). Then, P_i^{low}, I_i^{high}, and I_i^{low} are set to 430.75 kW ($=0.5 \times P_i^{\text{high}}$), 41.36 A (1.1 times of the rated current), and zero, respectively. As a result of the OCF, V_{RMSE} is minimized while the DGs satisfy the constraints as shown in Figure 6.

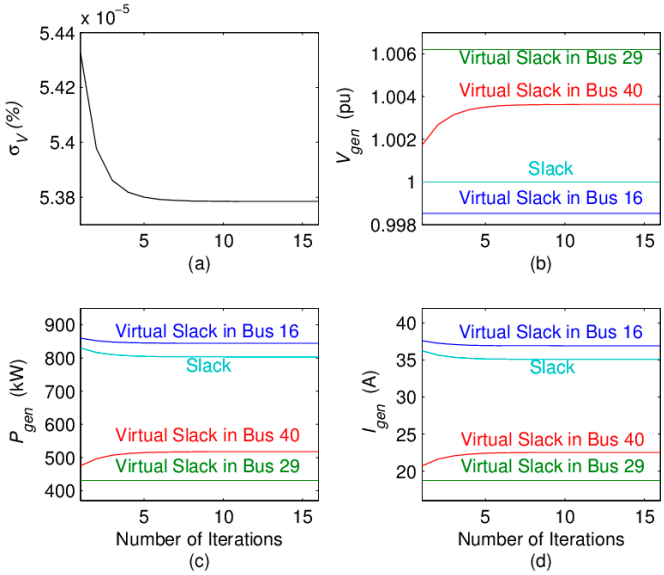

Figure 6. Result of optimal current flow analysis with constraints: (**a**) Root-mean-square- deviation of all bus voltages. (**b**) Voltages, (**c**) powers, and (**d**) currents of slack and virtual slacks.

The voltage in bus 29 is increased to prevent the power of the DG becoming smaller than P_{29}^{low}. In the same manner, the voltage in bus 16 is decreased to prevent the power of the DG becoming larger than P_{16}^{low}. As a result, all DGs secure sufficient margins to $P_i^{\max}$, so that they can emulate slack generators.

4.2. Virtual Slack Control Based on Current Sensitivity

4.2.1. Sensitivity to Errors Caused by Biased Measurement

To verify the regulation performance, which is described in Section III-*B*, 1% of the error is applied to the measurements in buses 16 and 40. In other words, the DGs in the buses 16 and 40 measure 1.01 and 0.99 times voltages/currents, respectively. As shown in Table 2, the current error is larger than 58% when the DG operates in the voltage control mode. In contrast, it is at most about 1% when the DG operates in the current control mode. The maximum voltage error is about 1% with the voltage control. In contrast, it is 0.05% with the current control.

Table 2. Voltage and current errors of DGs corresponding to control targets with 1% of measurement errors in buses 16 and 40.

		Ideal	Voltage Control		Current Control	
		Value (kV, A)	Value (kV, A)	Error (%)	Value (kV, A)	Error (%)
Bus 16	**V**	22.876	22.651	−0.98	22.872	−0.02
	I	37.286	17.882	−52.04	36.916	−0.99
Bus 29	**V**	23.042	23.037	−0.02	23.033	−0.04
	I	18.660	18.671	0.06	18.660	0
Bus 40	**V**	22.982	23.224	1.05	22.993	0.05
	I	22.648	35.938	58.68	22.877	1.01

4.2.2. Performance of Virtual Slack Control

In practice, the proposed current control method requires communication to receive the measured load currents and to send the current references to DGs. Therefore, there is a time delay before the DGs respond to the load changes. To reflect the delay, the data update interval is set to one second considering the existing energy management system (EMS) of the real power system. To emulate load variations, each load is randomly changed ten times per second within 1%/s. The performance of the virtual slack is verified with electromagnetic transient (EMT) simulations for an hour. For testing in harsh condition, the virtual slack is controlled based on the current sensitivity without the application of the OCF. As representatively shown in Figure 7, numerous simulations generally result in less than 1% of voltage variations with the virtual slack DGs, which share the load variation with the physical slack and the other virtual slack DGs as shown in Figure 8. The voltage variations become much larger without the virtual slack control as shown in Figure 9. This is because the only physical slack DG takes the charge of the load variations by itself as shown in Figure 10.

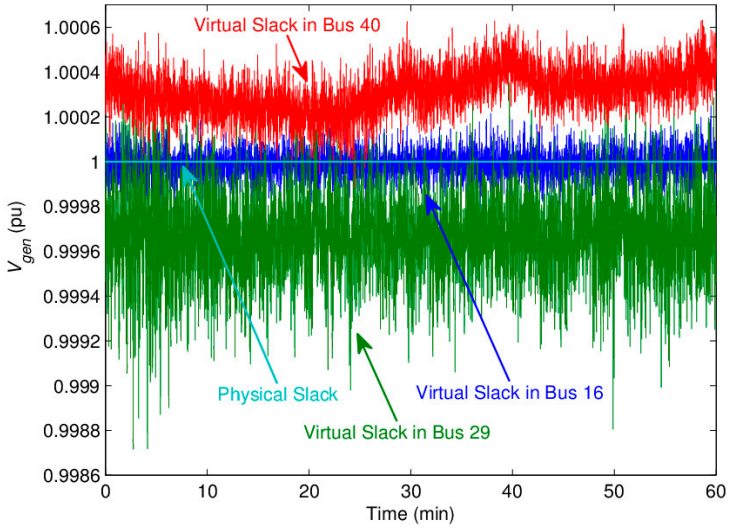

Figure 7. Voltages of physical and virtual slack distributed generations (DGs).

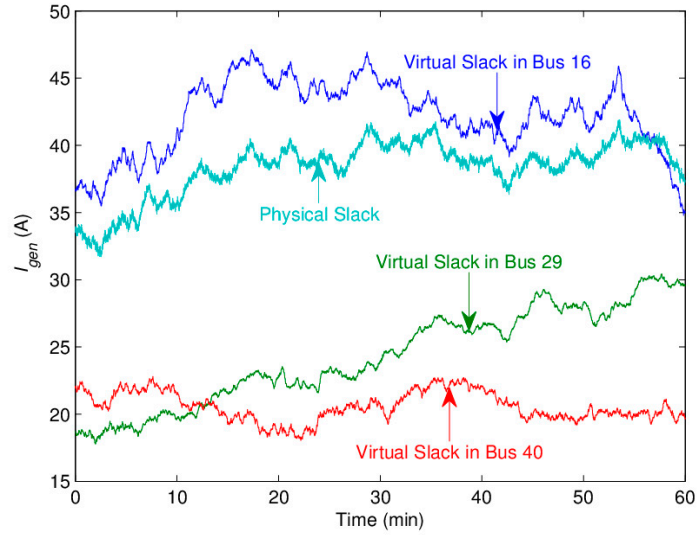

Figure 8. Currents of physical and virtual slack DGs.

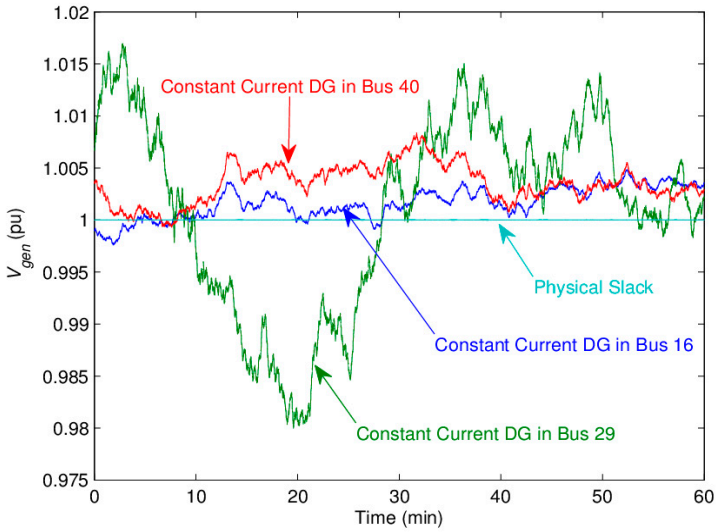

Figure 9. Voltages of physical slack and constant current controlled DGs.

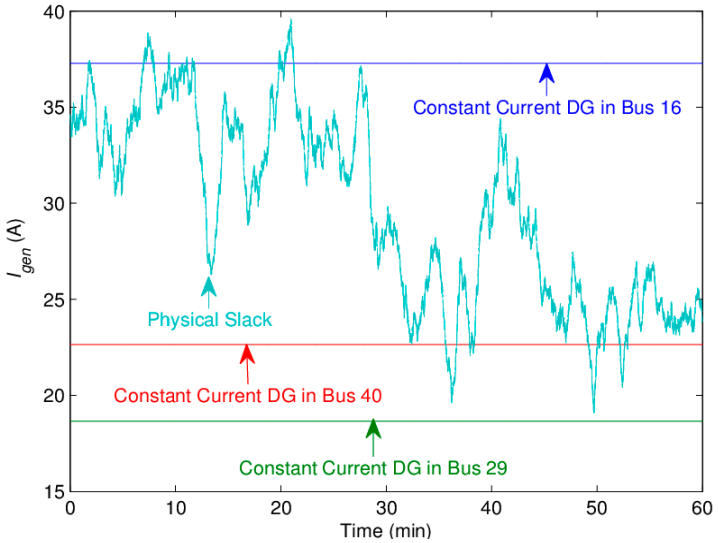

Figure 10. Currents of physical slack and constant current controlled DGs.

4.2.3. Operation by OCF and Virtual Slack Control

In practice, the members of the virtual slack DGs can be changed due to the operation mode change of the individual DG. This changes $\mathbf{R}_{gen}$ and $\mathbf{R}_{gen,row}$ in (31), and therefore, $\partial \mathbf{I}_{gen,ref}/\partial \mathbf{I}_L$ in Figure 4 must be updated. To verify the OCF, it is considered that the DG in bus 40 loses virtual slack control at 25 min. Obviously, the DG in bus 40 does not control its voltage, but it maintains its current in constant as shown in Figures 11 and 12, respectively. Remark that the DG in bus 16 also loses its voltage control at 25 min and restores that at 35 min by the OCF update. The virtual slack control effectively reduces the voltage variation even if a DG accidently loses its virtual slack control (see Figures 9 and 11). This is because the DGs still controls their currents based on the current droops before the OCF update. In short, the virtual slack control and the OCF improve voltage stability together.

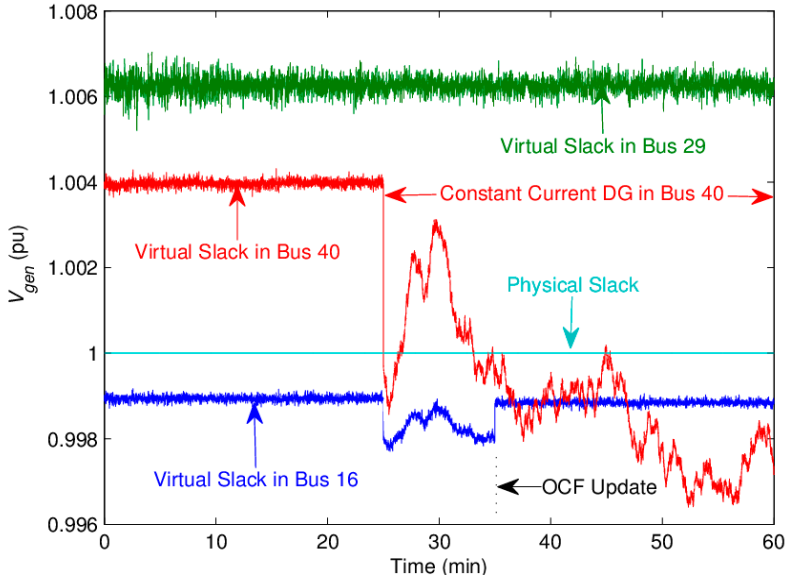

Figure 11. Voltages according to losing slack control and optimal current flow (OCF) update.

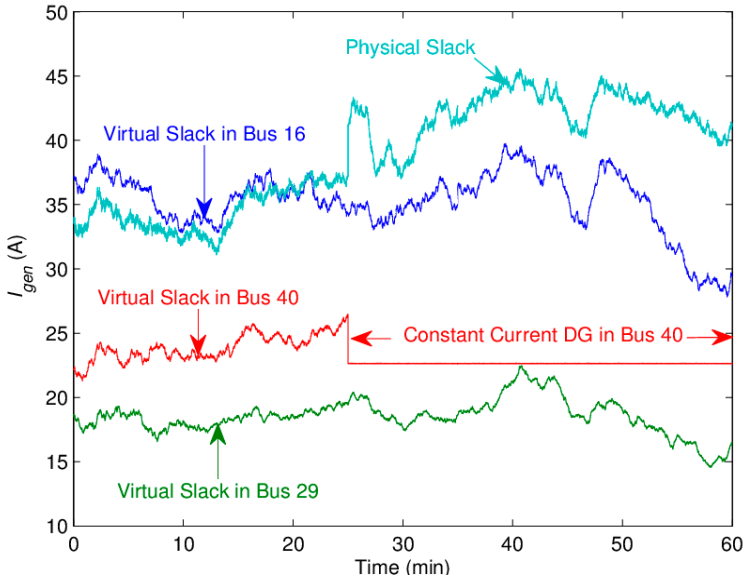

Figure 12. Currents after losing slack control in bus 40.

4.3. On-Line Estimation

The initial estimated conductance matrix is calculated using given line resistances. To reflect the errors between the given and the real values, at most 1% random noises are added to the given ones.

Then, the estimated conductance matrix is being updated on-line using V^{meas} and I^{meas} in (39) and (40). To obtain V^{meas} and I^{meas}, the DC distribution system is analyzed without the noise addition to the resistances, and then at most 0.1% random noises are added to the analyzed voltages and currents. To evaluate the estimation performance, V^{cal} and I^{cal} of (39) and (40) are calculated using the estimated conductance matrix. The on-line estimation performance is evaluated by applying at most 10% random errors to the line resistances at 10^4 seconds. The on-line estimation tunes the DC distribution system model both before and after the event as shown in Figure 13. The error comes from the imperfect given values of resistances. The on-line update of the root mean square error (RMSE) traces helps the decision making of the operator person who ultimately decides whether reflects the estimated value to the model.

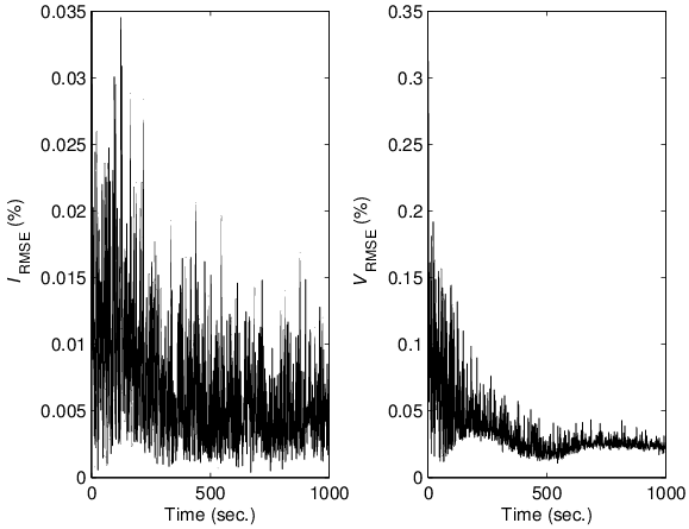

Figure 13. Root mean square errors (RMSEs) of currents and voltages from estimated conductance matrix.

5. Conclusions

This study proposed a virtual slack control based on the adaptive droop. In other words, voltages of the DC distribution system controlled accurately via the droop based current control. Therefore, it cleared both disadvantages of the direct DC voltage control and constant current (or power) control. The accuracy of the droop depends on the accuracy of the system conductance matrix, which was estimated on-line by the Kalman-filter algorithm. As a result, the voltage variation reduced to less than one fourth of the conventional system by applying the proposed control.

The result of this study might contribute to the distribution and expansion of DC devices, such as photovoltaic, fuel cell, battery energy storage system, electronic loads, etc.

Funding: This work was supported in part by Korea Electric Power Corporation (grant number: R18XA06-80).

Acknowledgments: This work was supported in part by Korea Electric Power Corporation (grant number: R18XA06-80).

Conflicts of Interest: The authors declare no conflict of interest.

References

1. Xu, L.; Chen, D. Control and Operation of a DC Microgrid with Variable Generation and Energy Storage. *IEEE Trans. Power Deliv.* **2011**, *26*, 2513–2522. [CrossRef]
2. Chang, Y.C.; Liaw, C.M. Establishment of a Switched-Reluctance Generator-Based Common DC Microgrid System. *IEEE Trans. Power Electron.* **2011**, *26*, 2512–2527. [CrossRef]
3. Baran, M.E.; Mahajan, N.R. DC Distribution for Industrial Systems: Opportunities and Challenges. *IEEE Trans. Ind. Appl.* **2003**, *39*, 1596–1601. [CrossRef]

4. Li, Y.; Luo, L.; Rehtanz, C.; Ruberg, S.; Yang, D.; Xu, J. An Industrial DC Power Supply System Based on an Inductive Filtering Method. *IEEE Trans. Ind. Electron.* **2012**, *59*, 714–722. [CrossRef]
5. She, X.; Huang, A.Q.; Lukic, S.; Baran, M.E. On Integration of Solid-State Transformer with Zonal DC Microgrid. *IEEE Trans. Smart Grid* **2012**, *3*, 975–985. [CrossRef]
6. Albu, M.; Kyriakides, E.; Chicco, G.; Popa, M.; Nechifor, A. Online Monitoring of the Power Transfer in a DC Test Grid. *IEEE Trans. Instrum. Meas.* **2010**, *59*, 1104–1118. [CrossRef]
7. Liu, B.; Liang, C.; Duan, S. Design Considerations and Topology Selection for DC-Module-Based Building Integrated Photovoltaic System. In Proceedings of the IEEE Conference on Industrial Electronics and Applications, Singapore, 3–5 June 2008; pp. 1066–1070.
8. Wu, T.F.; Chang, C.H.; Lin, L.C.; Yu, G.R.; Chang, Y.R. DC-Bus Voltage Control with a Three-Phase Bidirectional Inverter for DC Distribution Systems. *IEEE Trans. Power Electron.* **2013**, *28*, 1890–1899. [CrossRef]
9. Hayashi, Y. Approach for highly efficient and ultra compact converters in next generation 380 V DC distribution system. In Proceedings of the IEEE Energy Conversion Congress and Exposition, Raleigh, NC, USA, 15–20 September 2012; pp. 3803–3810.
10. Rodriguez, M.; Stahl, G.; Corradini, L.; Maksimovic, D. Smart DC Power Management System Based on Software-Configurable Power Modules. *IEEE Trans. Power Electron.* **2013**, *28*, 1571–1586. [CrossRef]
11. Majumder, R.; Ghosh, A.; Ledwich, G.; Zare, F. Power Management and Power Flow Control with Back-to-Back Converters in a Utility Connected Microgrid. *IEEE Trans. Power Syst.* **2010**, *25*, 821–834. [CrossRef]
12. Byeon, G.; Yoon, T.; Oh, S.; Jang, G. Energy Management Strategy of the DC Distribution System in Buildings Using the EV Service Model. *IEEE Trans. Power Electron.* **2012**, *28*, 1544–1554. [CrossRef]
13. Lu, D.D.C.; Agelidis, V.G. Photovoltaic-Battery-Powered DC Bus System for Common Portable Electronic Devices. *IEEE Trans. Power Electron.* **2012**, *24*, 849–855. [CrossRef]
14. Wang, C.M.; Lin, C.H.; Yang, T.C. High-Power-Factor Soft-Switched DC Power Supply System. *IEEE Trans. Power Electron.* **2011**, *26*, 647–654. [CrossRef]
15. Stupar, A.; Friedli, T.; Minibock, J.; Kolar, J.W. Towards a 99% Efficient Three-Phase Buck-Type PFC Rectifier for 400-V DC Distribution Systems. *IEEE Trans. Power Electron.* **2012**, *27*, 1732–1744. [CrossRef]
16. Kim, J.G.; Kim, S.K.; Park, M.; Yu, I.K.; Lee, H.; Kim, Y.G.; Kim, H.M.; Won, Y.J.; Jeong, K.W.; Yang, B. Loss Characteristic Analysis of HTS DC Power Cable Using LCC Based DC Transmission System. *IEEE Trans. Appl. Super Conduct.* **2012**, *22*, 5801304.
17. Marnay, C.; Lanzisera, S.; Stadler, M.; Lai, J. Building Scale DC Microgrids. In Proceedings of the IEEE Energytech, Cleveland, OH, USA, 29–31 May 2012; pp. 1–5.
18. Cvetkovic, I.; Dong, D.; Zhang, W.; Jiang, L.; Boroyevich, D.; Lee, F.C.; Mattavelli, P. A Testbed for Experimental Validation of a Low-voltage DC Nanogrid for Buildings. In Proceedings of the IEEE Power Electronics and Motion Control Conference, Novi Sad, Serbia, 4–6 September 2012; pp. LS7c.5-1–LS7c.5-8.
19. Willis, H.L. Analytical Methods and Rules of Thumb for Modeling DG-Distribution Interaction. In Proceedings of the IEEE PES Summer Meeting, Seattle, WA, USA, 16–20 July 2000; pp. 1643–1644.
20. Ochoa, L.F.; Feltrin, A.P.; Harrison, G.P. Time-Series-Based Maximization of Distributed Wind Power Generation Integration. *IEEE Trans. Energy Convers.* **2008**, *23*, 968–974. [CrossRef]
21. Falaghi, H.; Haghifam, M.R. ACO Based Algorithm for Distributed Generation Sources Allocation and Sizing in Distribution Systems. In Proceedings of the IEEE Lausanne Power Tech, Lausanne, Switzerland, 1–5 July 2007; pp. 555–560.
22. Shaaban, M.F.; Saadany, E.F.E. Optimal allocation of renewable DG for reliability improvement and losses reduction. In Proceedings of the IEEE Power and Energy Society General Meeting, San Diego, CA, USA, 22–26 July 2012; pp. 1–8.
23. Hadian, A.; Haghifam, M.R.; Zohrevand, J.; Rezai, E.A. Probabilistic Approach for Renewable DG Placement in Distribution Systems with Uncertain and Time Varying Loads. In Proceedings of the IEEE Power & Energy Society General Meeting, Calgary, AB, Canada, 26–30 July 2009; pp. 1–8.
24. Lee, S.H.; Kang, Y.C.; Park, J.-W. Optimal Operation of Multiple DGs in DC Distribution System to Improve System Efficiency. *IEEE Trans. Ind. Appl.* **2016**, *52*, 3673–3681. [CrossRef]
25. Saadat, H. *Power System Analysis*; McGraw Hill: Singapore, 2004; pp. 233–234.
26. Wilamowski, B.M.; Yu, H. Improved Computation for Levenberg- Marquardt Training. *IEEE Trans. Neural Netw.* **2010**, *21*, 930–937. [CrossRef] [PubMed]

27. Kamen, E.W.; Su, J.K. *Introduction to Optimal Estimation*; Springer: London, UK, 1999; pp. 149–183.
28. Lee, S.H.; Park, J.W. Selection of Optimal Location and Size of Multiple Distributed Generations by Using Kalman Filter Algorithm. *IEEE Trans. Power Syst.* **2009**, *24*, 1393–1400.